RESEARCH ARTICLE

3D-Printed Gelatin-Alginate Hydrogel Dressings for Burn Wound Healing: A Comprehensive Study

Fateme Fayyazbakhsh[1,2]*, Michael J. Khayat[3], Ming C. Leu[1,2]

[1]Department of Mechanical and Aerospace Engineering, Missouri University of Science and Technology, Rolla, Missouri, United States
[2]Intelligent System Center, Missouri University of Science and Technology, Rolla, Missouri, United States
[3]Department of Materials Engineering, McGill University, Montréal, Quebec, Canada

Abstract: Burn wound treatment is still a clinical challenge due to the severity of tissue damage and dehydration. Among various wound dressings, hydrogel materials have gained significant attention for burn wound treatment in clinical practice due to their soothing and moisturizing activity. In this study, 3D-printed dressings were fabricated using clinically relevant hydrogels for deep partial-thickness burn (PTB) wounds. Different ratios of gelatin and alginate mixture were 3D-printed and examined in terms of rheological behavior, shear thinning behavior, mechanical properties, degradation rate, and hydration activity to tune the hydrogel composition for best functionality. The cell-laden dressings were bioprinted to evaluate the effect of the gelatin: alginate ratio on the proliferation and growth of human dermal fibroblasts. The present findings confirm that the higher alginate content is associated with higher viscosity and Young's modulus, while higher gelatin content is associated with faster degradation and higher cell viability. Together, the 3D-printed dressing with 75% gelatin and 25% alginate showed the best tradeoff between mechanical properties, hydration activity, and *in vitro* biological response. Findings from *in vivo* test using the most effective dressing showed the positive effect of 3D-printed porous pattern on wound healing, including faster wound closure, regenerated hair follicles, and non-traumatic dressing removal compared to the non-printed hydrogel with the same composition and the standard of care. Results from this research showed that 3D-printed dressings with an adequate gelatin: alginate ratio enhanced wound healing activity for up to 7 days of moisture retention on deep PTB wounds.

Keywords: Burn wound; Moist wound healing; Advanced dressings; 3D printing; Gelatin; Alginate

***Correspondence to:** Fateme Fayyazbakhsh, 316 Engineering Research Lab, 500 West 16th Street, Rolla, Missouri 65401, USA; f.fba@mst.edu

Received: June 15, 2022; **Accepted:** July 21, 2022; **Published Online:** September 19, 2022

Citation: Fayyazbakhsh F, Khayat MJ, Leu MC. 2022. 3D-printed gelatin-alginate hydrogel dressings for burn wound healing: A comprehensive study. *Int J Bioprint*, 8(4): 618. DOI: http://doi.org/10.18063/ijb.v8i4.618

1. Introduction

Burn wound is one of the most challenging and debilitating wound types leading to significant disability, morbidity, and mortality[1]. There is ~1% of the global burden of diseases related to burns, leading to more than 9 million injuries and 120,000 deaths in 2017[2,3]. Approximately 1.1 million Americans suffer from burn injuries that require medical attention, accounting for over 60% of the acute hospitalizations in the United States[4,5]. Burn wound healing is a complex and delicate molecular-cellular process for restoring skin functions and repairing tissue damage[6,7]. Autologous skin grafts are still the gold standard for full-thickness burn treatment in clinical practices, while the current standard of care for deep partial-thickness burns (PTB) includes petrolatum gauze, topical antimicrobial agents, contact dressings, and hydrogels[8]. However, limitations such as prolonged healing, pain, traumatic removal, poor mechanical stability, limited body movement, scarring, and poor regeneration of skin appendages have fostered the development of dermal tissue engineering (DTE) solutions as an advanced approach to wound healing[9-13]. The desired features for burn wound dressings are considered to be antimicrobial, soothing, tunable water absorption/release, easy to remove, and transparent[14]. It is also a key feature for burn wound dressings to provide a non-adhesive contact that is elastic enough to support

body movement with no pain or trauma in the wound site.

Hydrogels are an essential class of polymers for dermal/epidermal regeneration (ER) due to their ability to donate and absorb water based on the wound condition. DTE mainly involves biodegradable hydrogels to encourage wound healing process within a moist environment[9,15]. Since 1977 when hydrogels were introduced as wound dressings for the 1st time[16], they have been developed from single-component hydrogels to complex compounds reinforced with nanoparticles, peptides, and growth factors[17]. Gelatin and alginate have been investigated for wound healing in various forms such as amorphous gels and films, mostly for wet and exuding wounds. Gelatin accelerates the inflammatory response and healing process by regulating macrophages and providing arginine–glycine–aspartic acid (RGD) sequences, and sodium alginate facilitates autolytic debridement[18-20]. Finding the adequate alginate-gelatin ratio in a hydrogel blend for wound dressing is critical to the success of wound healing, since gelatin and alginate have different mechanical, gelation, and biological properties due to the structural difference. To the best of our knowledge, despite the wealth of literature on the use of gelatin-alginate compounds as wound dressings, only one study evaluated different ratios of gelatin: alginate for burn wound healing[21]. In 2020, Afjoul *et al*.[21] examined freeze-gelled highly porous gelatin-alginate dressings with a 3% w/v concentration for second-degree burn wound treatment, which exhibited fast degradation and high swelling ratio not indicated for burn wound healing. The application of gelatin and alginate hydrogels for burn wound dressing is limited by fast degradation, short-term fixity, and traumatic adherence to the wound bed. These shortcomings can be addressed by increasing the concentration of gelatin-alginate in the hydrogel blend and using different fabrication methods such as 3D printing to develop hydrogel dressings with controlled pore size, tunable water absorption/donation, and improved fixity on the wound.

Over the last decade, skin bioprinting as an extension of 3D printing has been widely investigated to develop various tissue engineering constructs for artificial skin, synthetic grafts, and wound dressings. Skin 3D bioprinting allows for the reproducible fabrication of various bioinks and cells with precise control over the structure, geometry, mechanical properties, and functionality of the graft or dressing[22-25]. Researchers mainly focused on developing 3D bioprinted skin grafts using various materials and cells[26-28], rather than developing 3D-printed wound dressings specifically for burn wounds[29]. The majority of prior research on 3D-printed wound dressings has focused on developing absorbent dressings for wet/exuding wounds and chronic wounds with moderate to high exudation rather than burn wound healing, which requires continuous hydration instead of moisture absorption. To meet the specific needs of burn wound that vary with wound size, depth, and patient condition, 3D printing has the capability to fabricate personalized wound dressings[29]. The first attempt at developing 3D-printed dressings for burn wound treatment was published in 2021 by Teoh *et al*.[29]. They used extrusion-based 3D printing to develop personalized wound dressings with chitosan methacrylate loaded with different drugs and antimicrobial agents for burn wound treatment. To the best of our knowledge, no previous research has investigated 3D-printed dressings with different ratios of gelatin and alginate blend for burn wound treatment, and the effect of gelatin: alginate ratio on printing outcome and functionality of the 3D-printed dressings has remained unclear. Furthermore, there is a need for deeper evaluation of therapeutic efficacy of the 3D printing technology considering the known benefits of non-printed gelatin-alginate hydrogels in burn wound treatment. The current research investigates the effect of gelatin: alginate ratio on printing outcome and hydration activity, as a specific need of burn wound treatment. We highlight in the present paper the therapeutic effect of 3D printing technology by comparing 3D-printed dressings with non-printed hydrogel dressing of the same composition.

In this study, 3D-printed acellular dressings with different ratios of gelatin and alginate were fabricated and characterized for further enhancement of burn wound care products. To tune the gelatin: alginate ratio at a favorable level for 3D printing, the rheological behavior and shear thinning behavior of the hydrogels were measured. Mechanical properties, degradation rate, and hydration activity were measured to relate the functionality of the 3D-printed dressings with gelatin: alginate ratio. MTT and Live/Dead assays were used to evaluate the biocompatibility of the dressings using human dermal fibroblasts (HDF). An *in vivo* wound healing study was conducted using the most effective dressing in terms of stiffness, hydration activity, and cell viability on deep PTB wound in a rat model. The wound healing activity of the most effective 3D-printed dressing was compared with non-printed hydrogels of the same formulation and petrolatum gauze, which served as the control group.

2. Materials and methods

2.1. Materials

Gelatin type B (from porcine skin), sodium alginate, calcium chloride anhydrous, Dulbecco's Modified Eagles Medium (DMEM), fetal bovine serum (FBS), 1%

penicillin/streptomycin (pen/strep), MTT, and trypsin/EDTA were purchased from Sigma-Aldrich (St. Louis, MO, USA). All materials were used as received without further modification.

2.2. Bioink preparation

First, the stock solutions of gelatin and alginate were prepared separately by dissolving 0, 200, 400, 600, and 800 mg of each powder in 10 mL deionized water to obtain 0, 2, 4, 6, and 8 w/v% of each hydrogel. The schematic microstructure of gelatin and alginate is shown in **Figure 1**. The hydrogels were filtered and stirred at 600 rpm at 40°C for 30 min to obtain clear homogenous hydrogel solutions. Alginate was added to the stirring gelatin solution dropwise to obtain gelatin-alginate hydrogel mixtures with a total concentration of 8 w/v%, as shown in **Table 1**. To print the cell-laden dressings, 10^5 cells/mL of the primary (HDF, ScienCell Research Laboratories, CA, USA) were centrifuged and suspended in DMEM and added to the stirring gelatin solution at 37°C. Then, the alginate solution was added dropwise. The hydrogels were poured into plastic cartridges for 3D printing. The cartridges were centrifuged at 300 rpm for 1 min to remove the air bubbles and then stored at 4°C. All the materials and equipment were autoclaved or sterilized with UV light before the experiments.

2.3. 3D printing

We adopted the extrusion-based 3D printing technology as a low-temperature bioprinting modality using the Inkredible®bioprinter (CELLINK Corporation, Sweden). The dressings were printed directly onto sterile Petri dishes with the print head and print bed temperature adjusted at 22 – 23°C and 15°C, respectively. The dressings were printed at 2.5 mm/s speed in square and dog bone geometries at 20 × 20 × 3 mm^3 and 30 × 10 × 5 mm^3 dimensions, respectively, for different testing setups.

Table 1 shows the composition and printing parameters for each hydrogel. To improve the mechanical properties, the 3D-printed dressings were immersed in calcium chloride ($CaCl_2$) 0.2 M solution for 10 min to form cross-links between alginate chains. The cross-linked 3D-printed dressings were washed with deionized water 3 times to remove the excessive Ca ions. The 3D-printed dressings were stored at 4°C for further use. **Figure 2** shows the bioink preparation and 3D printing process.

2.4. Structural and physicochemical characterization

2.4.1. Rheological behavior and viscosity measurement

The rheological behavior of the hydrogels was measured before 3D printing. All rheology tests were performed by

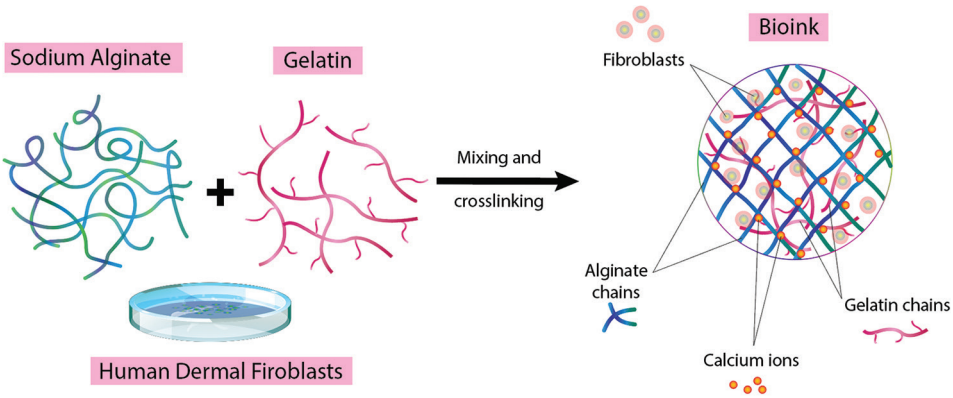

Figure 1. Schematic of the structure of sodium alginate, gelatin, and gelatin-alginate blend in 3D-printed cell-laden dressings. Gelatin and alginate are semi-interpenetrating networks (semi-IPN), whereby the linear chains of alginate are embedded within the gelatin network, which decreases the free volume[39].

Table 1. Gelatin-alginate hydrogel compositions and printing parameters

Hydrogel composition (in 10 mL deionized water)	Sample code	Nozzle inner diameter (mm)	Extrusion pressure (kPa)	Print head temperature (°C)
8 w/v% gelatin	G8-A0	0.337	40±10	22
6 w/v% gelatin+2 w/v% alginate	G6-A2	0.337	50±10	22.5
4 w/v% gelatin+4 w/v% alginate	G4-A4	0.26	80±10	22.5
2 w/v% gelatin+6 w/v% alginate	G2-A6	0.26	80±10	22.5
8 w/v% alginate	G0-A8	0.26	100 ± 20	23

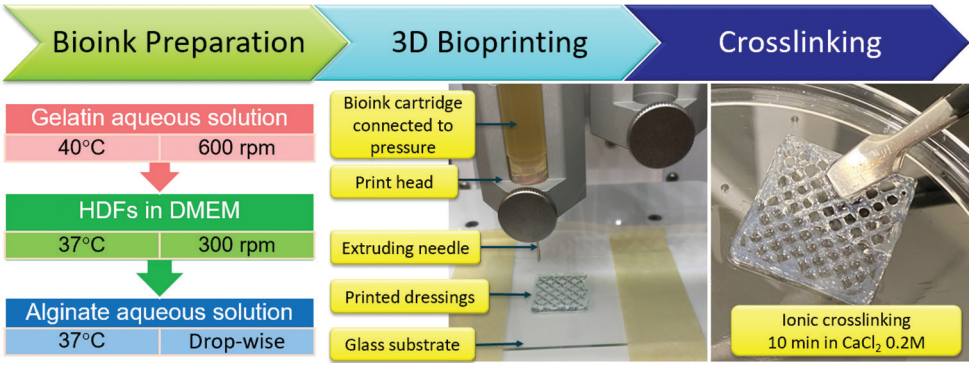

Figure 2. Fabrication of 3D-printed wound dressings with alginate, gelatin, and human dermal fibroblasts for partial-thickness burn wounds followed by 10 min crosslinking with calcium chloride solution.

a Rheometer (HAAKE™ MARS™, Thermo Scientific, MA, USA) using a parallel plate (diameter = 35 mm) setup with a frequency of 1 Hz and a gap of 1 mm at 22°C for 300 s. All measurements were performed within the linear viscoelastic region. To relate the rheological behavior and bioink composition, the storage modulus and loss modulus (G' and G", respectively) were analyzed for the various gelatin: alginate ratios.

The viscosity and shear thinning behavior of the non-printed hydrogels with different ratios of gelatin and alginate were measured by a rotational rheometer (Kinexus, Ultra+, Malvern Instruments Ltd., UK) using a parallel plate setup for shear rate ramp test with a 0.5 mm gap at 22°C. The tests were conducted using a solvent trap to avoid drying during the test. To relate the shear thinning behavior and bioink composition, the shear stress, shear strain, and shear rate were measured for the various gelatin: alginate ratios.

2.4.2. Mechanical testing

A uniaxial tensile test was performed on the dog-bone-shaped scaffolds of dimensions 25 × 50 × 1 mm^3 in accordance with the ASTM F2150-8 standard. Young's moduli of the 3D-printed scaffolds were measured using the Universal Instron 5969 Dual Column Testing System (Instron, MA, USA) and the BlueHill Universal Software system (n = 3). The scaffolds were assessed using a mechanical load frame at a speed of 5 mm/min typical for polymer specimens to measure the modulus of elasticity, yield strength, and yield strain of the scaffolds.

2.4.3. Fourier-transform infrared spectroscopy (FTIR)

A Nicolet iS50 FTIR spectrophotometer (Thermo Scientific, MA, USA) equipped with a diamond crystal cell of attenuated total reflection accessory in the mid-IR region (4000 – 400 cm^{-1}). All the spectra were recorded at a resolution of 4 cm^{-1} with 32 scans with a data spacing of 0.482 cm^{-1}. 500 µL of each hydrogel sample were loaded on the beam splitter area to make a thin film on the crystal. A fresh reference spectrum was recorded after every five scans and deducted from the obtained spectra. All the recorded spectra were analyzed with OMNIC 9.2.41 software (Thermo Scientific, MA, USA), and data showed as Transmittance (%) against wavenumber (cm^{-1}). The IR Spectrum data from Sigma Aldrich were used to identify characteristic chemical bonds in gelatin, alginate, and water.

2.5. Swelling capacity and biodegradation rate measurement

To determine the further interactions between the wound and dressing, the swelling capacity and the degradation rate of the 3D-printed dressings were recorded after soaking in phosphate-buffered saline (PBS). Samples were dried at room temperature, and the dry weight of the samples was recorded as W_D (n = 3). Then, the samples were immersed in 3 mL PBS at 32°C to reach equilibrium swelling and subsequent degradation. The weight changes in determined time intervals were recorded for up to 7 days as the dressings will stay on the wound for up to 7 days. The dressing's swelling capacity and degradation rate were calculated using the following equations:

$$Swelling\ capacity(\%) = \frac{W_{max} - W_D}{W_D} \times 100 \quad (1)$$

$$Degradation\ rate(mg\ /\ min) = \frac{W_D - W_{Week1}}{7 \times 24 \times 60} \quad (2)$$

where W_D is the initial dry weight, W_{max} is the maximum weight of the scaffolds after immersion, and W_{week1} is the weight after 1 week of immersion in PBS.

2.6. Hydration activity test

To measure the effect of gelatin: alginate ratio on hydration activity, firstly, the total amount of water in each 3D-printed scaffold was measured using thermogravimetric analysis on 250°C for 10 min (SDT Q600 V20.9 Build 20, Universal V4.5A TA Instruments,

USA). The weight change was considered as the total water content (n = 3)[30].

To predict the hydration activity of the samples on burn wounds, ethylcellulose super absorbent foam (Shield Line LLC, NJ, USA) was used as a model of the dehydrated burn wound. The 3D-printed dressings were mounted on the foam surface at 32°C, and hydration activity was calculated by weight change after 24 h. It is highly important to provide continuous hydration in the first 24 h after injury, because the systemic capillary leak, intravascular fluid loss, and large fluid shifts will mostly occur within the first 24 h, peaking at around 6 – 8 h after injury[31,32]. The total water content and moisturizing activity were calculated using the following equations:

$$Total\ water\ content\ (\%) = \frac{W_0 - W_H}{W_0} \times 100 \quad (3)$$

$$Moisturizing\ activity = \frac{(W_0 - W_{24})}{W_0 - W_H} \quad (4)$$

where W_0 is the initial weight, W_H is the weight after heating at 250°C, and W_{24} is the weight after placing on dry surfaces for 24 h.

2.7. *In vitro* biological evaluation

2.7.1 MTT assay

MTT assay was used to test and compare the viability and proliferation of dermal cells after exposure to the 3D-printed acellular dressings. In this research, the sample extracts were used to indirectly evaluate the cell viability in accordance with the ISO-10993 standard. The extracts were collected and filtered after 3, 7, and 14 days of immersion of the 3D-printed dressing in DMEM (3 replications). The DMEM culture media with no further treatment were considered as the control sample. First, HDF cells were cultured in 100 µL DMEM plus 10% FBS and 1% pen/strep (10^4 cells/well) and incubated at 37°C with 5% carbon dioxide (CO_2). After 24 h, the initial culture media were replaced by 90 µL sample extract fortified with 9% FBS plus 1% pen/strep. After 24 h, the media were replaced by 100 µL MTT 0.5 M solution. After 4 h, the MTT solution was replaced by 100 µL isopropanol. After 30 min, the optical density (OD) of formazan crystals was read at 545 nm using an ELISA reader (Stat Fax 2100, USA).

2.7.2. Live/dead assay

Live/Dead assay was used to assess the direct cell viability of the 3D-bioprinted dressings using HDFs. Therefore, the 3D-bioprinted cell-laden dressings were evaluated in direct contact with HDF cells (n = 3). Non-printed hydrogels were mixed with 10^5 cells/mL and consequently bioprinted under aseptic conditions. The bioprinted cell-laden scaffolds were placed in 6-well plates and maintained in 5 mL DMEM fortified with 5% FBS and 1% Pen/Strep. Blank wells cultured with HDFs with no further treatment were considered as the control samples. After 3 days of incubation at 37°C, the cell-laden scaffolds were exposed to the Live/Dead staining kit (Abcam, MA, USA) for 10 min according to the manufacturer's manual. The viable and dead cells within the samples were observed using a confocal microscope (Nikon, Japan) in green and red channel, respectively. The live and dead cell counts were measured using ImageJ software v1.53s (National Institute of Health, MD, USA).

2.8. Animal test

2.8.1. In vivo burn wound model

All *in vivo* experiments were approved by the Institutional Animal Care and Use Committee at the Missouri University of Science and Technology (Reference No. 177-20). The ability of the 3D-printed wound dressings for the treatment of deep PTB wound healing was evaluated by creating a circular burn wound using a hot metal bar on the lumbar area of 18 Sprague Dawley rats, in three groups of six rats in each group (n=6), as follows:

i. Control: Wounds covered with petrolatum gauze as the current standard of care
ii. Non-printed hydrogel: Wounds covered with non-printed hydrogel
iii. 3D-printed hydrogel: Wounds covered with 3D-printed hydrogel dressings.

After shaving the animal's back area, the skin was cleaned with iodine and then sterilized with alcohol swabs. The animals were anesthetized using inhaled isoflurane through a nose cone. The deep partial-thickness defect was made by placing a 100°C metal bar of 20 mm diameter on the lumbar area of the rat for 10 s. After implementation, the wounds were disinfected by Dermoplast antiseptic spray (Advantice Health LLC, NJ, USA). After applying the treatment, the wounds were covered with Petrolatum Gauze and Elastikon bandage (3M, MN, USA). **Figure 3** shows the application of dressing on the wounds in the three groups. All animals were monitored for post-operative recovery on a daily basis, and the wounds were inspected under isoflurane anesthesia every week to record the change in wound size and formation of necrotic tissue formation. Sharp debridement was performed and recorded if needed. The experiment was terminated after 4 weeks by euthanizing the animals using a lethal dose of CO_2. Wound tissue explants were incised and fixed in formalin solution overnight for further histology investigation.

2.8.2. Wound closure

Dermal wounds were photographed every week after removing the old dressing and before rebandaging, to track the wound size, color, necrotic tissue formation, and any trauma caused by dressing removal. A sterile disposable ruler was inserted close to the wound as the scale. The wound size was quantified by tracing the wound border in each photograph using ImageJ software. The wound closure was calculated as follows:

$$Wound\ closure\,(\%) = \frac{A_0 - A_t}{A_0} \times 100 \qquad (5)$$

where A_0 is the wound area immediately after wound implementation, and A_t is the wound area at time t (i.e., 1, 2, 3, and 4 weeks). Traumatic removal was evaluated by assessing the presence of traumatic laceration, bleeding, and redness in wound margins and surrounding tissues after the dressing removal.

2.8.3. Histology analysis

Wound tissue explants (25 × 25 mm^2) were resected and fixed overnight in 10% neutral buffered formalin, then cut into 1 mm thickness tissue blocks that include wound tissues, margins, and surrounding tissues. Tissue blocks were processed and embedded in paraffin using a fully automated tissue processor (TissueTek 2000, Sakura Finetek, CA, USA). Tissue blocks were sectioned at 5 μm and mounted on positively charged glass slides for staining with hematoxylin and eosin (H&E). The slides were imaged using a transmitted light bright field microscope (Olympus BX53 microscope fitted with an Olympus DP70 digital camera) using the ×4 and ×10 objective lenses. The entire tissue section was scanned, digitally photographed, and "photomerged" to form a single composite image using Adobe Photoshop (Adobe, CA, USA). Quantitative histomorphometry was performed by measuring the epidermal layer, dermal layer, and granulation tissue (GT) thickness. H&E-stained sections were blindly graded by two trained graders with sections scored on a scale of 0 – 4 in terms of ER, dermal regeneration (DR), and GT thickness[33], as depicted in **Table 2**. ImageJ and Adobe Photoshop software were used for histomorphometric evaluations and tissue slide photo merging.

2.9. Statistical analysis

All experimental results were reported as the means ± SD of at least three replications for each sample per test. Statistical significance was determined using one-way ANOVA and Student's *t*-test with ($P < 0.05$) as the level of significance.

3. Results and discussion

3.1. Rheological behavior and shear thinning behavior

An important question associated with hydrogel 3D printing is the effect of rheological properties on printability. Printable materials ideally enable the consistent flow and reproducible fabrication. Viscosity has been widely reported as the determinant factor of printability in viscoelastic materials, for example,

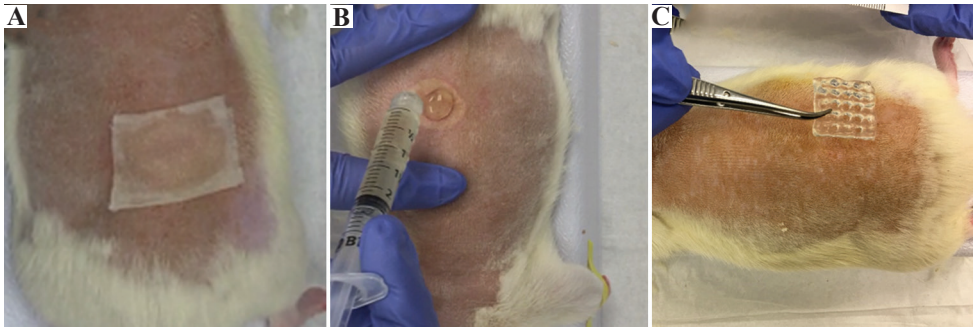

Figure 3. Animal test for the evaluation of deep partial-thickness burn wound healing using a rat model in three groups. Burn wounds covered with (A) petrolatum gauze, (B) non-printed hydrogel, and (C) 3D-printed hydrogel dressings.

Table 2. Qualitative histological grading criteria adopted from Altavilla *et al*.[33]

Score	Epidermal regeneration	Dermal regeneration	Granulation tissue thickness
0	No epidermal organization	No dermal organization	Very thin or no granular layer
1	Very little epidermal organization	Very little dermal organization	Thin granulation layer
2	Little epidermal organization	Little dermal organization	Moderate granulation layer
3	Moderate epidermal organization	Moderate dermal organization	Thick granular layer
4	Complete remodeling of epidermis	Complete remodeling of dermis	Very thick or no granular layer

hydrogels. Due to the complexity of shear modulus in viscoelastic materials, this parameter is described by two distinct dynamic modulus components including storage modulus (G') and loss modulus (G"), which are associated with elastic and viscous behavior, respectively. The rheological behavior of the non-printed gelatin-alginate hydrogels was studied to relate the bioink composition with the shear modulus. As shown in **Figure 4A**, the alginate content dominantly affects both complex viscosity and elasticity, as by increasing the alginate content from 0 to 8 w/v%, both G' and G" increased. This is associated with the relatively higher molecular weight and polarity of functional groups in alginate chains and the higher fluctuation of the intramolecular non-covalent bonds in gelatin chains[34]. Our observation is consistent with that reported in Gao *et al*.[35]. The increase in G' and G" requires the extrusion pressure to increase, as shown in **Table 1. Figure 4B** shows the shear thinning behavior of the hydrogels. G6-A2 showed the highest shear thinning, followed by G4-A4 and G2-A6. Plain gelatin and plain alginate showed the lowest shear thinning behavior. The shear thinning results suggest that hydrogel blend exhibits higher shear thinning behavior due to increased electrostatic interaction between gelatin and alginate chains and decreased free volume. **Figure 5** shows the

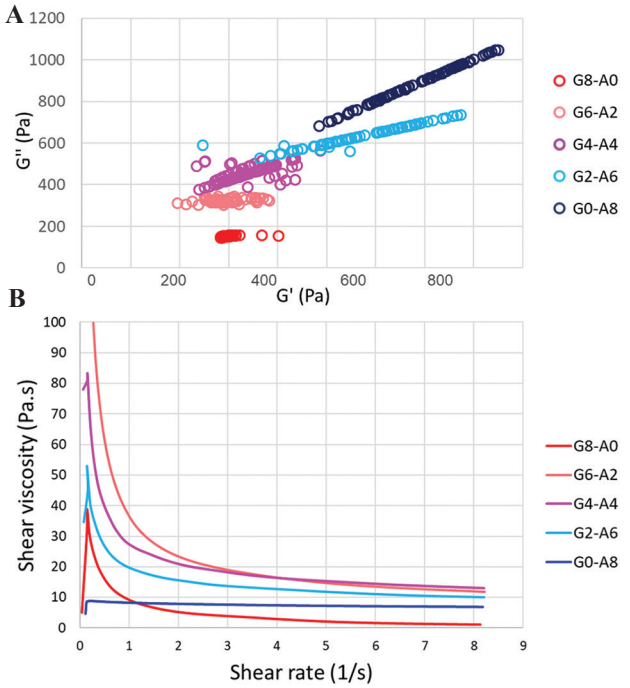

Figure 4. (A) Complex shear moduli (G' and G") of the non-printed hydrogels. Alginate content is associated with higher G' and G", (B) shear thinning behavior of the non-printed hydrogels. Plain alginate and plain gelatin showed the lowest shear-thinning behavior, while G6-A2 exhibited the greatest shear-thinning behavior followed by G4-A4 and G2-A2.

3D-printed dressings in a square grid pattern. G0-A8 and G2-A6 showed poor post-printing shape fidelity, suggesting that higher alginate content not only requires higher printing pressure but also decreases the pore shape fidelity compared to samples with lower alginate content. G4-A4 dressing showed the finest mesh structure and best shape fidelity, followed by G6-A2. The nozzle diameter is one of the most important printing parameters directly affecting the printing outcome[36]. Initially, all samples were printed using the same nozzle size. However, as shown in **Table 1**, larger nozzle diameters were used to print G6-A2 and G8-A0, as these samples showed inconsistent extrusion with smaller nozzles, while G4-A4, G2-A6, and G0-A8 showed consistent extrusion with the smaller nozzle. G2-A6 and G0-A8 showed poor shape fidelity, even with the smaller nozzle size due to higher viscosity and lower shear thinning behavior in these samples. The better shape fidelity in the G4-A4 over G6-A2 hydrogel results from (i) higher shear thinning behavior, as shown in **Figure 4B**, (ii) using a smaller nozzle that increases the extrusion accuracy in G4-A4, and (iii) desired electrostatic interactions between gelatin and alginate chains as semi-interpenetrating network (semi-IPN) hydrogel blends. The physical entanglement of alginate chains within the ample free volume in gelatin network increases the electrostatic interactions in the hydrogel blend, as shown in **Figure 1**. The G8-A0 hydrogel showed poor printability and irregular pore shape due to the low viscosity and poor shear thinning behavior (**Figure 4B**), high chain fluctuation at room temperature, and inconsistent extrudability even with the larger nozzle size.

The required energy for hydrogel extrusion is associated with the length of polymeric chains, that is, the molecular weight. The molecular weight of gelatin ranges from 50 to 100 kDa with very low extensibility of the network and high entropy in 22 – 23°C, which justifies the relatively low viscosity and elasticity of gelatin[37]. Alginate consists of linear pleated chains of mannuronic acid and guluronic acid, as depicted in **Figure 1**. Sodium alginate with higher mannuronic acid to guluronic acid (M: G) ratio shows lower gelation with better extrudability than calcium alginate, which is in the sol state[38]. The G8-A0 sample, that is, the plain gelatin, is classified as a temperature-sensitive hydrogel with relatively low viscosity, which is not ideal for extrusion-based 3D printing. The superior extrudability and printability of the G4-A4 and G6-A2 dressings are associated with the higher chemical interactions between the amine groups in gelatin and the carboxylate and hydroxyl groups in alginate. The physical entanglement in the hydrogel blend reduces the free volume at a molecular level. The linear cationic chains in alginate occupy the free volume in the gelatin network, making the hydrogel

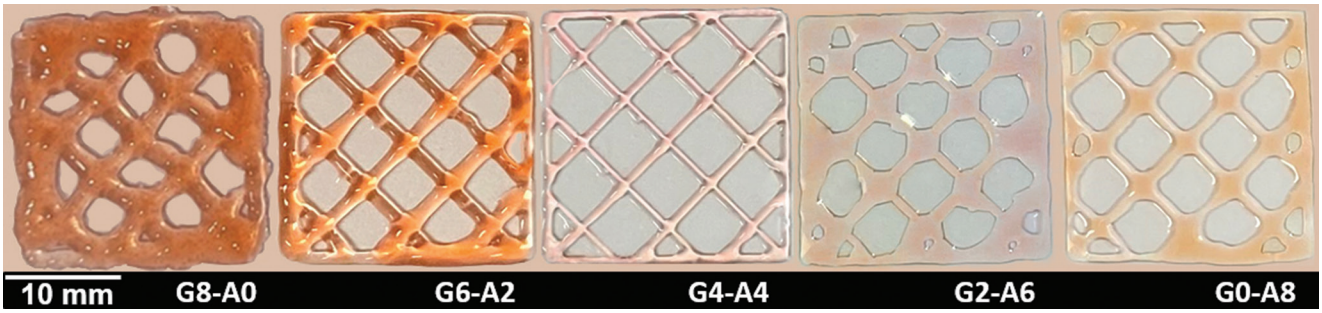

Figure 5. Photographs of the 3D-printed dressings. G4-A4 and G6-A2 dressings showed the finest mesh structure and best shape fidelity. The G8-A0 showed poor printability and inconsistent pore shape fidelity, while G2-A6 and G0-A8 samples were too viscous and difficult to extrude with irregular pore shape and size.

blend denser and more consistent, as both gelatin and alginate are semi-interpenetrating networks (semi-IPN), as depicted in **Figure 1**. In semi-IPN hydrogel blends, a linear or branched hydrogel is embedded within the other hydrogel network with or without crosslinking, which decreases the free volume. While in IPN hydrogels, two or more hydrogels cross-link in the presence of each other to form a 3D network with an increased free volume[39]. The lower free volume and higher consistency are responsible for enhanced flowability in the hydrogel mixture. Accordingly, the G6-A2 and G4-A4 hydrogel samples exhibit a good balance between viscosity and extrudability. Higher viscosity implies mixed effects on hydrogel printability, fror example, higher mechanical stability but lower printability due to the higher extrusion pressure required. Furthermore, higher extrusion pressure increases shear stress during printing, which is invasive to the cells. Shear stresses have been shown to induce morphological changes, cytoskeleton reorganization, and generation of reactive oxygen species, and alter gene and protein expression[37].

3.2. Mechanical properties

Many authors in the literature have discussed the effects of calcium ion exposure on sodium-alginate crosslinking and mechanical strength[25]. In this research, we cross-linked the 3D-printed dressings with different gelatin: alginate ratios to improve the mechanical strength. **Figure 6** shows Young's modulus of the 3D-printed dressings. It is important to highlight the fact that wound dressings are required to exhibit adequate tensile stiffness during the application, wearing, and removal to serve as a barrier against traumas and external pathogens. Furthermore, dressings should be adequately elastic to adapt to the wound surrounding tissues and body movement, that is, in the same range as normal skin[40]. The Young's modulus (E) of normal skin fluctuates between 0.42 MPa and 0.85 MPa[41]. The tensile testing results from this work strongly support the positive effect of alginate content on mechanical stiffness due to (i) stronger chemical

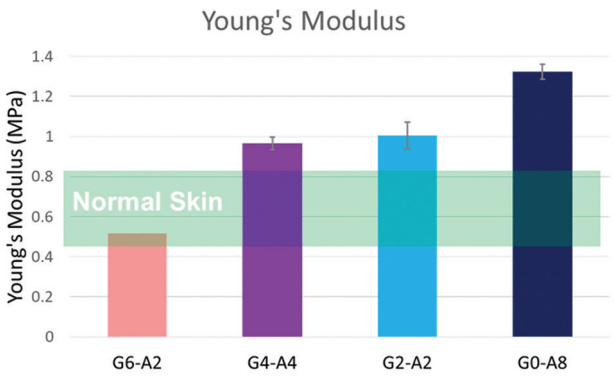

Figure 6. Young's modulus of 3D-printed dressings (n = 3). Mechanical stiffness is increased by alginate content; however, only G6-A2 samples are in the same range as normal skin. The Young's Modulus of the normal skin is adopted from[41]. Wound dressings need to have the stiffness matched with normal skin to support body movement, non-adhesive coverage, and persistence on the wound site. The mechanical properties of the plain gelatin dressing are not measurable.

bonds in post-printing alginate and (ii) a larger number of cross-links formed within the alginate network. It is generally accepted that the stronger chemical bonds in the hydrogel network result in higher mechanical strength and lower permeability. However, only the 3D-printed G6-A2 dressings exhibited Young's modulus in the range of the normal skin. Burn wound dressings must provide a non-adhesive surface that is elastic enough to support body movement with no pain or trauma in the wound site. Furthermore, an adequate mechanical stiffness is required to maintain the dressings fixed on the wound without falling apart. Therefore, the samples with Young's modulus matched with normal skin considered as best samples for further testing. It is notable that the dressings with lower stiffness will move on the wound surface during body movement, while dressings with higher stiffness compared to the skin will limit body movement causing stress shielding, secondary trauma, and skin tear on the wound site and surrounding tissues. The G8-A0 sample was excluded from experiment as the

mechanical properties of this sample is not measurable due to the lack of crosslinks.

3.3. Chemical structure

Notably, the hydrogel-based bioinks provide good permeability to oxygen and nutrients. FTIR spectroscopy was conducted to evaluate the interactions between the alginate and gelatin within the hydrogel blend. The IR spectra of the gelatin-alginate complex are shown in **Figure 7** in accordance with their structure, as shown in **Figure 1 and Figure 8A-B**. Alginate and gelatin have overlapping carboxylate groups and hydroxyl groups in different intensities associated with 3200 – 3500 cm^{-1} characteristic peaks. The amide bonds increase as the gelatin concentration increases, while at the same time, the carboxylate groups decrease as the concentration of alginate decreases, which is compensated by the rising gelatin content. Specifically, the spectrum of sodium alginate displayed the characteristic absorption bands of its polysaccharide structure at 1318 cm^{-1} (C–O stretching), 1126 cm^{-1} (C–C stretching), and 1021 cm^{-1} (C–O–C stretching). The absorption bands around 1620 and 1416 cm^{-1} are assigned to asymmetric and symmetric stretching peaks of the carboxylate groups in alginate[42-44].

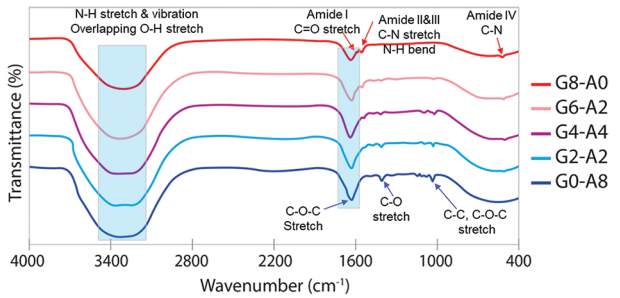

Figure 7. Fourier-transform infrared spectroscopy spectra of hydrogel samples. The characteristic IR bands associated with gelatin, sodium alginate, and water are shown by red arrows, blue arrows, and light blue boxes, respectively.

The FTIR spectrum of gelatin has the characteristic absorption bands at 1659 cm^{-1} (amide I, C–O, and C–N stretching), 1547 cm^{-1} and 1243 cm^{-1} (amide II and III, C–H stretching vibration, and N–H bending), and 601 cm^{-1} (Amide IV, C–N), respectively[45-47].

In the spectra of the alginate-gelatin complex in G6-A2, G4-A4, and G2-A6 samples, the stretching peak assigned with carboxylate groups of alginate slightly shifted to the left, which is due to the overlapping peaks of amide I and amide II peaks and the dominant absorption of water O-H scissors (1634 cm^{-1}) in this area. The formation of intermolecular hydrogen bonds between different functional groups in gelatin and alginate makes a favorable entanglement for enhanced rheological, shear thinning, and mechanical behavior at certain ratios of gelatin: alginate. However, after crosslinking the 3D-printed dressings, the formation of covalent cross-links between calcium ions and guluronic acid blocks in alginate results in lower permeability and higher mechanical stiffness[25].

3.4. Degradation rate and hydrating activity

Figures 9A and B depict the swelling and degradation profile of the 3D-printed dressings after immersing in PBS at 32°C. All samples showed swelling (i.e., water absorption) in the early 24 h, while G6-A2 dressings showed significantly higher swelling capacity than the other 3D-printed dressings. The higher swelling capacity of this sample is due to the higher water permeability of the gelatin chains, which is clearly associated with the low molecular weight and weak chemical bonds in the gelatin structure. After cross-linking, stronger chemical bonds will form within the alginate chains by exchanging the sodium ions with calcium ions. It is associated with a lower permeability to water molecules and, thus lower swelling in the alginate chain. Based on the same rationale, the degradation rate of the samples with higher gelatin content is significantly faster than the alginate chain. This is particularly important when investigating

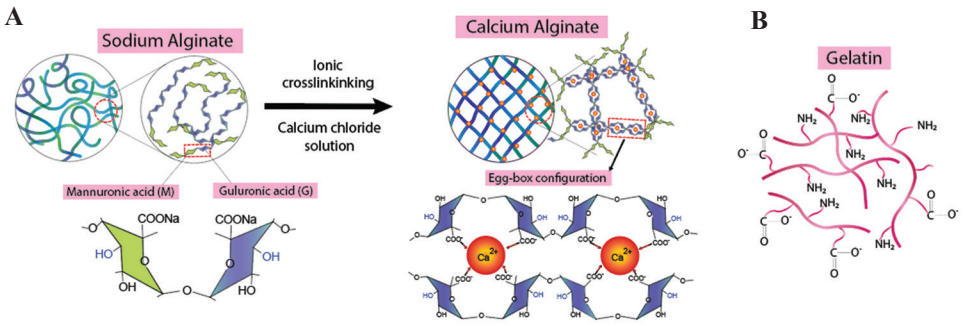

Figure 8. (A) Sodium alginate has linear chains composed of mannuronic acid and guluronic acid with carboxylate groups and hydroxyl groups. During cross-linking calcium ions replace the sodium ions in the guluronic acid monomers, resulting in intermolecular bonds between calcium ions and alginate chains that forms a linear and packed egg-box structure. (B) Gelatin is a bioactive derivative of collagen composed of amide groups with relatively high free volume and low viscosity.

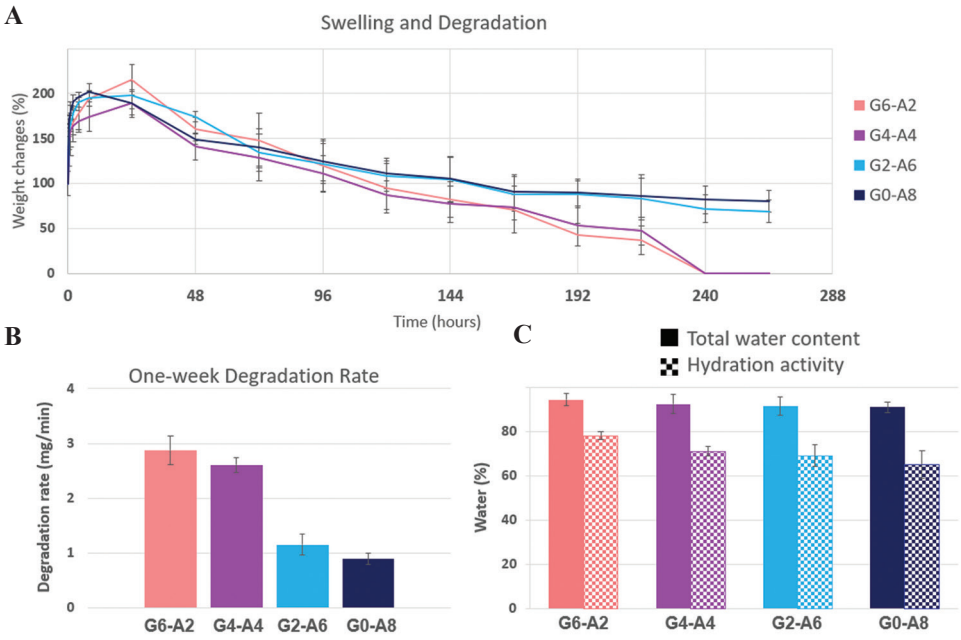

Figure 9. (A) Swelling capacity and degradation of the 3D-printed dressings ($n = 3$). (B) One-week degradation rate of 3D-printed dressings ($n = 3$). Samples with higher gelatin content showed a faster degradation rate and higher swelling capacity. All samples could stay in PBS for at least 7 days (168 h). The G6-A2 dressings with the highest gelatin content showed significantly faster degradation ($P < 0.05$), which means that the permeability of this sample is higher than the other samples. (C) Total water content and hydration activity of the gelatin-alginate 3D-printed dressing on a super-absorbent surface to simulate dry burn wound surface ($n = 3$, $P < 0.05$). The higher permeability in this sample justifies its faster degradation and higher water donation.

wound care products, as it is favorable for wound dressings to stay on the wound for 3 – 7 days to reduce the pain and discomfort to the patient, risk of infection, the trauma caused by dressing removal, and cost. All samples showed up to 7 days of persistence in PBS, which predicts the long-lasting persistence of the proposed dressings on the wounds. As shown in **Figure 9B**, the degradation rate in the 3D-printed dressing decreased by increasing the alginate concentration, which confirms the prolonged degradation of G0-A8 and G2-A6 due to the higher covalent cross-links in these samples. The results from swelling and degradation rate support the clinical stability of all dressings for 1-week wound coverage. The G6-A2 dressings showed the fastest and highest degradation associated with the acidic residues of the gelatin chain during the degradation, which can also accelerate the degradation of alginate chains. Furthermore, as shown in **Figure 9A and B**, the faster degradation rate and higher swelling capacity in G6-A2 dressing are associated with higher interaction with water molecules, which is a key factor for further biocompatibility. According to other studies, an acidic environment helps wound healing by controlling wound infection, antimicrobial activity, protease activity, and oxygen release[48,49]. Notably, the dressing samples with prolonged degradation that remains longer than 7 days on the wound are not recommended for burn wound healing due to the lower interactions with wound surface and prolonged healing that increase the infection risk and chronic wound incidence. Accordingly, the G6-A2 dressing with relatively higher gelatin content and adequate degradation rate will support burn wound healing more efficiently compared to the other samples.

We studied the water content and water donation ability of the 3D-printed dressings to predict their hydration activity for clinical burn wound healing. **Figure 9C** depicts the total water content and overnight water donation of the dressings on ethylcellulose substrate as a super-absorbent surface representing the dehydrated surface of burn wounds. The water content slightly increased by gelatin concentration, as G6-A2 dressings showed 94.3 ± 2.9% water content. Furthermore, by increasing the gelatin concentration, hydration activity is increased after overnight exposure to the ethylcellulose membrane as a burn wound model, which is due to the (i) lower degree of cross-linking, (ii) weaker chemical bonds, (iii) higher permeability, and (iv) lower molecular weight of gelatin network compared to alginate chains. This is consistent with the higher swelling capacity and faster degradation rate in the G6-A2 dressing. **Figures 8A and B** show the electrostatic interactions between the amide groups of gelatin and the carboxylate and hydroxyl groups of alginate, which are associated with the increased physical entanglement and the reduced free volume in the hydrogel mixture network, particularly in the G6-A2

and G4-A4 dressings. The lower free volume and higher entanglement are associated with higher consistency and flowability. It also justifies the lower viscosity and better shape fidelity outputs in G4-A4 and G6-A2 dressings, which have the most entanglement between the gelatin amide groups and alginate carboxylate/hydroxyl groups. These results collectively indicate the promising burn wound healing capacity of the G6-A2 dressing.

3.5. *In vitro* biological evaluation

The *in vitro* biocompatibility of 3D-printed gelatin-alginate dressings was evaluated by MTT assay and Live/Dead assay, using HDFs, as depicted in **Figures 10** and **11**. The viability and proliferation of HDF cells after 24 h of exposure to the dressings extracts were determined using an MTT assay after 1, 3, and 7 days to measure OD values. According to the MTT results, G6-A2 dressing showed slightly lower cell viability than the control group on days 1 and 3 ($P > 0.05$). On day 7, this sample exhibited the highest cell proliferation compared to the rest of the samples and the control group ($P < 0.05$). In contrast, when the alginate concentration was increased, cell viability decreased on days 1 and 3 compared to the control group. The gelatin concentration positively affects cell viability, as the amino acids in the gelatin chains provide a favorable matrix for cell attachment, resulting in increased cell proliferation in G6-A2 dressing compared to the other samples. Gelatin is a product of partial hydrolysis of collagen protein, which is the main protein of the dermal extracellular matrix (ECM). Hence, gelatin can provide the required ingredients for bioactive DR with no adverse immune response that justifies the positive effect of gelatin content on cell viability and biological response. More specifically, arginylglycylaspartic acid (arginine–glycine–aspartic acid, i.e., RGD) is the most common peptide motif responsible for cell adhesion to the ECM. Gelatin contains RGD peptide sequences, which are essential for stable communication between the cells and the surrounding ECM. The presence of amino acids and RGDs in the gelatin network provides favorable anchors for cell attachment and proliferation to enhance cell adhesion through interactions with integrin and fibronectin[50,51]. On day 7, 3D-printed G6-A2 dressings showed higher cell viability than the control group and other groups, which confirms the long-term cell viability of the G6-A2 dressings.

The Live/Dead assay results in **Figure 11** indicate only a few dead cells in G6-A2 cell-laden dressings, associated with higher RGD available in this dressing. However, this sample showed no significant difference in cell survival compared to the control group ($P > 0.05$). In contrast, it showed significantly higher cell viability and biocompatibility than the rest of the samples ($P < 0.05$). This is consistent with the findings of the MTT assay (**Figure 10**). Higher alginate concentration exhibits lower cell viability due to the lack of RGD sequences within the alginate chains. Accordingly, the G0-A8 and G2-A6 dressings were excluded from animal test due to the significantly lower cell viability.

In summary, the lower cell viability of samples with higher alginate content is associated with lack of RGDs and lower interaction with water molecules due to the lower free volume, stronger chemical bonds, and higher molecular weight of alginate compared to gelatin. For the same reason, samples with higher alginate content exhibit higher stiffness. In clinical practices, wound dressings are required to exhibit mechanical stiffness in the range of normal healthy skin to allow for painless body movement. Despite the superior extrudability of G4-A4 dressings, this sample is excluded from the further animal test due to the lower biocompatibility and higher stiffness compared to the normal skin.

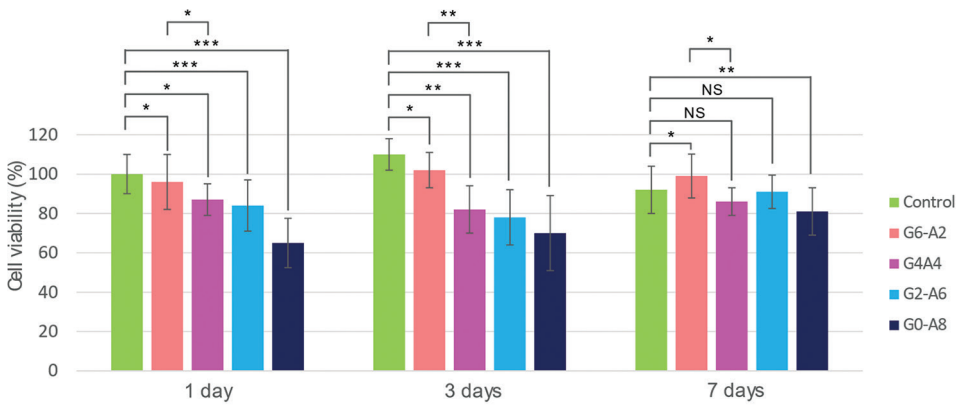

Figure 10. Indirect *in vitro* biological evaluation of the 3D-printed dressings. MTT assay results showed that cell viability and proliferation increased significantly by increasing the gelatin content. G6-A2 samples showed higher cell viability than the control group on day 7. ($n = 3$; *, **, ***, and NS denote $P < 0.05$, $P < 0.01$, $P < 0.001$, and non-significant difference, respectively).

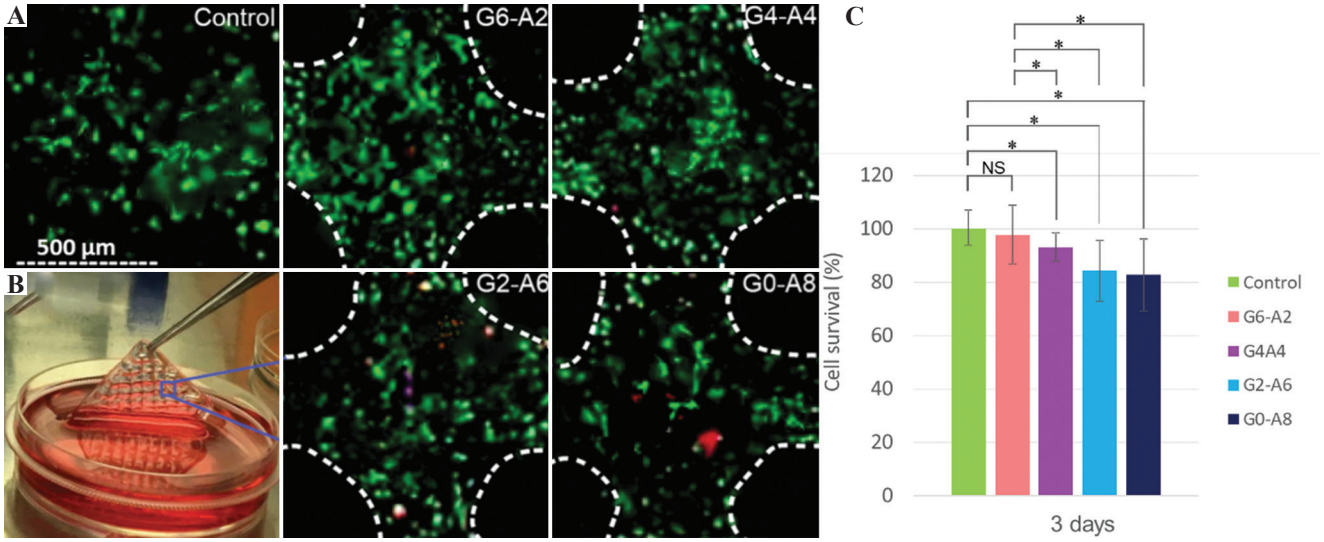

Figure 11. Direct *in vitro* biological evaluation of the 3D-printed dressings. (A) Live/Dead confocal images of cell-laden dressings after 3 days of culture. Living cells are depicted in green, while dead cells are depicted in red. (B) Cell-laden dressing cultured in Dulbecco's modified eagles medium for further Live/Dead assay. (C) Quantitative representation of cell viability based on the Live/Dead confocal images. Samples with higher gelatin content showed higher cell survival than those with higher alginate content. The G6-A2 dressings showed no significant difference with the control sample in terms of cell survival, while significantly higher cell survival compared to other samples. (n = 3, * and NS denote $P < 0.05$ and non-significant difference, respectively).

3.6. *In vivo* burn wound healing

To improve our understanding of the effect of 3D-printed dressings on wound healing, we applied the 3D-printed hydrogel dressings on burn wounds using a rat model. To meet the ethical issues associated with the animal tests, we performed the animal test only on one representative group (i.e., the best sample) as the treatment group. Although the G8-A0 showed the highest hydration activity and cell viability, it is excluded from animal testing due to its undesirable fast degradation time, lack of mechanical stability, and poor shape fidelity. As discussed, the G0-A8 and G2-A6 suffer from significantly lower cell viability, preventing the inclusion of these samples in the animal test. Despite the superior rheological behavior of G4-A4 dressings, it is associated with two major concerns: (i) mechanical stiffness out of the range of normal skin, which can cause pain and loss of fixity on the wound site, and (ii) significantly lower cell viability compared to the control sample ($P < 0.05$) and G6-A2 dressings. Overall, the 3D-printed dressing with 75% gelatin and 25% alginate (i.e., G6-A2) showed the best tradeoff between shape fidelity, hydration activity, and *in vitro* biological response. In addition, only this sample exhibited adequate mechanical stiffness matched with normal skin.

To differentiate the effect of 3D printing technology with hydrogel composition on wound healing activity, we examined non-printed G6-A2 against 3D-printed G6-A2. The *in vivo* burn wound healing efficacy of G6-A2 dressings in critical-sized deep PTB using an SD rat model in a 28-day experiment. Wounds were rebandaged and imaged every 7 days for 4 weeks. Wound images on days 0, 7, 14, 21, and 28 were analyzed to estimate the wound contraction ranging from the initial deep PTB of 20 mm diameter on day 0 to the full-wound closure on day 28. **Figure 12** shows the wound closure as the main characteristic of wound healing, indicating that the wound closure occurred significantly faster in both printed and non-printed hydrogel (3D-printed and non-printed G6-A2) than in the control group. The 3D-printed dressing showed slightly faster wound closure than the non-printed hydrogel with the same composition, and both showed significantly faster wound closure than the control group. **Table 3** compares the different parameters of wound treatment, including ease of use, necrotic tissue formation, and wound margins for treatment groups and control groups. Both treatment groups showed less necrotic tissue than the control group ($P < 0.05$), while the 3D-printed dressings showed better autolytic debridement with smoother wound margins that is less invasive, as shown in **Figure 12 and Table 3.** Furthermore, the dressing removal was less traumatic in 3D-printed dressings than in the non-printed hydrogel and the control group. In addition, the 3D-printed dressing group showed smoother wound margins, which results from more efficient hydration, as shown in **Figure 12 and Table 3**. The necrotic tissue is significantly lower in 3D-printed group compared to the control group at week 3 ($P < 0.05$). Furthermore, the necrotic tissue in 3D-printed group was automatically debrided without any sharp debridement or invasive removal of necrotic tissue. However, the control and non-printed hydrogel

groups required sharp instruments for the removal of necrotic tissue. The sharp debridement as an invasive procedure slows down the healing time and results in significant pain with further analgesia administration. The non-adhesive surface of the 3D-printed dressings keeps the surface from sticking to the wound, with no pain or harm to the GT or epithelialization during dressing removal. The non-printed hydrogel is required to be rinsed rigorously to clean the wound surface. The control dressing requires intensive force and sharp debridement to pull off from the wound surface, resulting in trauma, bleeding, and significant damage to the healing tissue. The porous surface and higher mechanical integrity of the 3D-printed dressings are associated with the autolytic debridement and non-adhesive surface of the dressings, as well as the continuous water donation that keeps the wound adequately moisturized. As discussed above, continuous hydration and autolytic debridement are two key features of burn wound treatment. As shown in **Figures 12-13 and Table 3**, the non-printed hydrogel group is not capable of continuous hydration due to the fast and uncontrolled release of water molecules in the first hours, which is due to the lack of crosslinks within the alginate chains as well as non-porous amorphous gel compared to the 3D-printed dressing group. The uncontrolled hydration activity causes wound maceration (i.e., excessive water absorption in the wound) with an elevated risk of infection, bacterial load, and wound dehydration after a few days[52,53]. Lack of continuous hydration in the non-printed treatment group indicates that this sample cannot adequately moisturize the wound for 7 days. The dry surface of petrolatum gauze in the

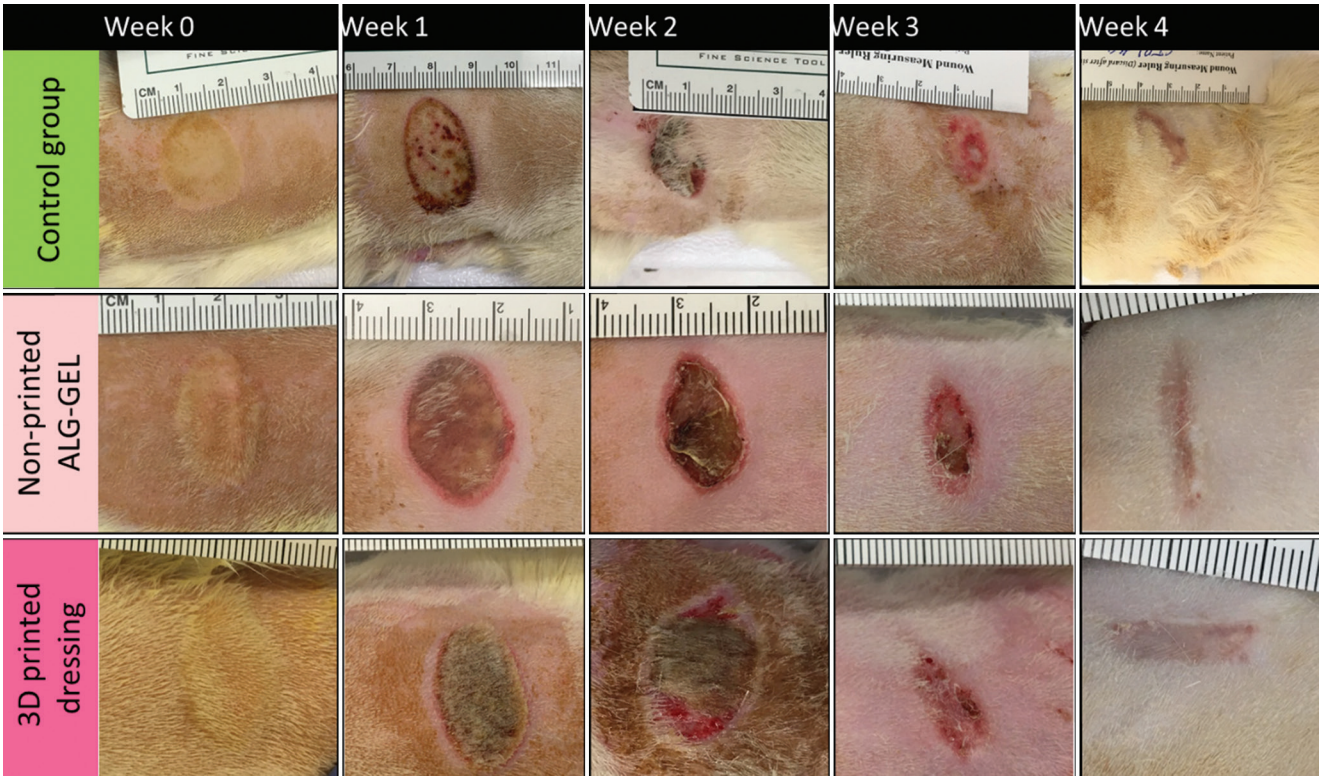

Figure 12. Wound healing analysis over 4 weeks (n = 6). Gross examination of wound healing. Wound images from control and treatment groups. 3D-printed dressings showed less necrotic tissue and smoother wound margins.

Table 3. Comparison between treatment groups and control group

Dressing group	Dressing application	Dressing removal	Moist wound healing	Secondary trauma	Necrotic tissue	Autolytic debridement	Sharp debridement	Wound margin
Control	Easy	Very sticky	Not seen	Extremely	>50%	Not seen	required	Thick crust
Non-printed hydrogel	Easy	Sticky	Yes, short-term	Slightly	<10%	Partially	Partially required	Sloping
3D-printed dressing	Easy	Easy	Yes, continuous	Not seen	Not seen	Yes	Not required	Smooth, flat

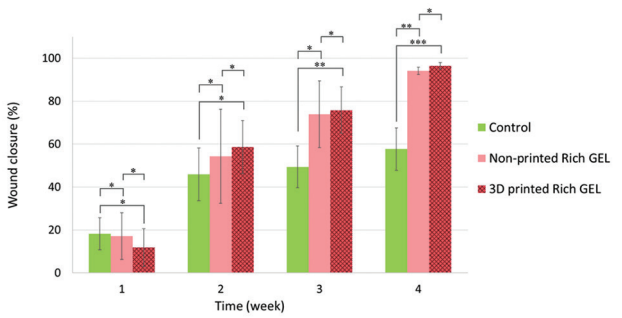

Figure 13. 3D-printed dressings and non-printed G6-A2 dressings with 75% gelatin and 25% alginate showed significantly higher wound closure (i.e., smaller wound size) than the control sample, while the printed dressing showed slightly higher wound closure than the non-printed dressing. (n = 3; *, **, and *** denote $P < 0.05$, $P < 0.01$, and $P < 0.001$, respectively).

control group cannot support the burn wound hydration and only keeps it from infection and water loss due to evaporation, which confirms the low healing capacity of the standard of care in the group compared to the proposed treatment ($P < 0.05$).

Figures 14A-C show representative H&E-stained slides for the 3D-printed dressings, non-printed dressings, and control groups. **Figure 15** depicts the average score of ER, DR, and GT formation as the main indicators of wound healing. The control group showed the lowest ER with the thickest hyperkeratosis, as shown in **Figure 14A**. GT formation after 28 days is a major indication of immature wound healing, and it showed the highest level in the control sample. More specifically, GT refers to the chronically vascularized tissue that represents the persisted inflammation, mainly composed of pink and granular tissue with macrophages and proliferating fibroblasts[54]. The persistence of GT until week 4 represents immature healing and failed treatment. As shown in **Figures 14A-C**, the control sample shows considerable GT formation, while both non-printed and 3D-printed dressings show slight GT formation compared to the control group. On the other hand, the 3D-printed dressing showed a distinctive formation of hair follicles due to the continuous hydration and non-stick surface with aligned pores. The number of hair follicles (green arrowheads) is significantly higher in the 3D-printed hydrogel than in the non-printed hydrogel and the control group. Furthermore, the hair follicles in the 3D-printed group showed significantly higher growth from the dermal layer to the epidermal layer and beyond that, while in the non-printed hydrogel dressing and the control group, hair follicles are still in the dermal layer, which means the growth and development of hair follicles began after 4 weeks. In the same line, more sweat glands and skin appendages (white arrowheads) were regenerated

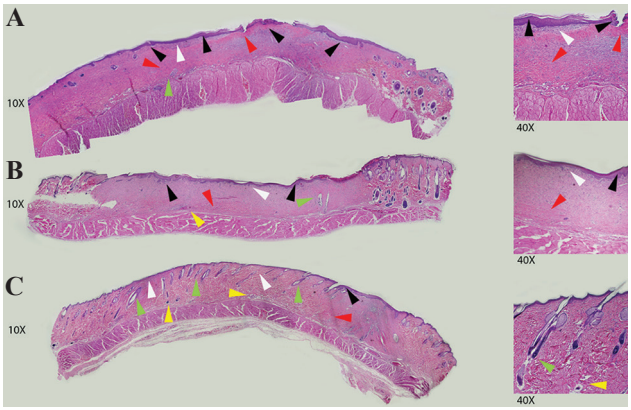

Figure 14. Representative H&E-stained slides for (A) control group: burn wound covered with petrolatum gauze, (B) wound covered with non-printed amorphous hydrogel composed of 75% gelatin and 25% alginate (G6-A2), (C) wounds covered with 3D-printed G6-A2. Pop-outs are regions of interest for further magnification. Guide: hyperkeratosis (black arrowhead), epidermal regeneration (dark purple outmost layer), dermal layer (white arrowhead), granulation tissue (red arrow), hair follicle (green arrowhead), and sweat glands (yellow arrowhead) labeled in the images.

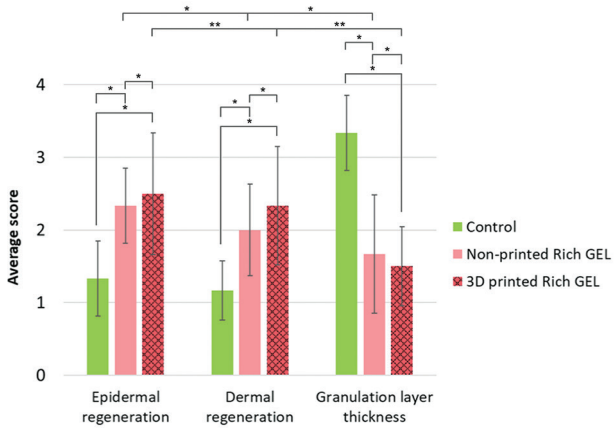

Figure 15. Gross histology results based on the H&E grading scores (**Table 3**) regarding epidermal regeneration, dermal regeneration, and granulation tissue formation. The control group showed insufficient epidermal and dermal regeneration with the thickest granulation layer as an indicator of immature tissue treatment, while the 3D-printed dressing showed significantly higher regeneration of hair follicles. (n = 6; * and ** denote $P < 0.05$, $P < 0.01$, and $P < 0.001$, respectively).

in all groups, with slightly higher regeneration in the 3D-printed dressing group. Overall, the *in vivo* results provide evidences for the positive effects of 3D-printed dressings on burn wound healing that comes from the increased degradation rate, mechanical strength, and contact surface, along with the well-studied wound healing activity of gelatin-alginate hydrogels as water reservoir with favorable amino acids sequences within the hydrogel network.

The results from this study provide substantial evidences on the effects of gelatin: alginate ratio on printability and mechanical properties. As discussed, alginate content showed positive effects on flowability, shape fidelity, and mechanical stiffness due to the higher molecular weight of alginate and the formation of crosslinks within the alginate network. Accordingly, gelatin content positively affected degradation rate and hydration activity due to the lower molecular weight and higher permeability. Furthermore, gelatin content is associated with higher cell viability and proliferation due to the amino acid sequences, specifically RGDs as a favorable anchor for cell attachment. Overall, the 3D-printed dressing with 6 wt/v% gelatin and 2 w/v% alginate showed the best balance among shape fidelity, mechanical properties matched with normal skin, hydration activity, and *in vitro* biological response. We examined 3D printing and hydrogel composition as two independent variables to more accurately judge the proposed dressings on deep PTB wound treatment. The 3D-printed dressings showed faster wound closure and lower wound contracture than the non-printed hydrogel with the same composition and the standard of care, that is, petrolatum gauze.

4. Conclusion

In this study, we proposed hydrogel wound dressings based on different gelatin: alginate ratios that can be fabricated and customized using 3D printing technology. The present findings confirm that the higher alginate content is associated with higher viscosity and tensile stiffness, while the higher gelatin content is associated with faster degradation and higher cell viability. Together, the 3D-printed dressing with 75% gelatin and 25% alginate showed the best tradeoff among shape fidelity, mechanical stiffness matched with normal skin, hydration activity, and *in vitro* biological response. The findings from *in vivo* burn wound healing show evidence of the positive effects of 3D-printed dressings on wound healing compared to non-printed hydrogels. Overall, the outcome of this study provides promising insights for using bioink formulations toward 3D printing technology as a versatile approach to tissue engineering and regenerative medicine. The results of this research can also help further research on more complicated bioinks incorporated with nanoparticles, growth factors, and bioactive reagents by providing details on the gelatin-alginate interactions as a tunable combination of printability and bioactivity. We envision that 3D-printed gelatin-alginate bioinks can be further extended through the other aspects of skin bioprinting by incorporation of stem cells and other signaling factors to facilitate scarless wound healing and regeneration of skin appendages not only for burn wound treatment, but also for other complex chronic ulcers such as diabetic foot ulcers and vascular ulcers as well as to develop skin models for pharmaceutical and cosmetic industries.

Acknowledgment

The authors wish to express sincere thanks to Drs. Delbert Day, Yue-wern Huang, Anthony Convertine, Douglass Bristow, Nathan Leigh, Richard Watters, and Baojun Bai for their consultation advice and infrastructure support.

Funding

This work was funded by Midwest Biomedical Accelerator Consortium (MBArC), an NIH Research Evaluation and Commercialization Hub (REACH), and by Ozark Biomaterial Initiative.

Conflict of interest

The authors declare that they have no competing interests.

Author contribution

Conceptualization: Fateme Fayyazbakhsh, Ming C. Leu
Data curation: Fateme Fayyazbakhsh, Michael J. Khayat
Formal analysis: Fateme Fayyazbakhsh, Michael J. Khayat
Funding acquisition: Fateme Fayyazbakhsh, Ming C. Leu
Methodology: Fateme Fayyazbakhsh
Investigation: Fateme Fayyazbakhsh, Ming C. Leu
Project administration: Ming C. Leu
Writing – original draft: Fateme Fayyazbakhsh
Writing – review and editing: Ming C. Leu.

References

1. Kowal S, Kruger E, Bilir P, *et al*., 2019, Cost-effectiveness of the Use of Autologous Cell Harvesting Device Compared to Standard of Care for Treatment of Severe Burns in the United States. *Adv Ther*, 36:1715–29. https://doi.org/10.1007/s12325-019-00961-2
2. James SL, Lucchesi LR, Bisignano C, *et al*., 2020, Epidemiology of Injuries from Fire, Heat and Hot Substances: Global, Regional and National Morbidity and Mortality Estimates from the Global Burden of Disease 2017 Study. *Inj Prev*, 26:i36–45. https://doi.org/10.1136/injuryprev-2019-043299
3. Price K, Lee KC, Woolley KE, *et al*., 2021, Burn Injury Prevention in Low-and Middle-Income Countries: Scoping Systematic Review. *Burns Trauma*, 9:tkab037. https://doi.org/10.1093/burnst/tkab037
4. Zavlin D, Chegireddy V, Boukovalas S, *et al*., 2018, Multi-

institutional Analysis of Independent Predictors for Burn Mortality in the United States. *Burns Trauma*, 6:24. https://doi.org/10.1186/s41038-018-0127-y

5. Yu TC, Zhang X, Smiell J, *et al*., 2020, Healthcare Resource Utilization, Treatment Patterns, and Cost of Care Among Patients with Thermal Burns and Inpatient Autografting in Two Large Privately Insured Populations in the United States. *Burns*, 46:825–35. https://doi.org/10.1016/j.burns.2019.10.019
6. Gonzalez AC, Costa TF, Andrade ZD, *et al*., 2016, Wound Healing a Literature Review. *An Bras Dermatol*, 91:614–20. https://doi.org/10.1590/abd1806-4841.20164741
7. Han G, Ceilley R, 2017, Chronic Wound Healing: A Review of Current Management and Treatments. *Adv Ther*, 34:599–610. https://doi.org/10.1007/s12325-017-0478-y
8. Dhaliwal K, Lopez N, 2018, Hydrogel Dressings and their Application in Burn Wound Care. *Br J Community Nurs*, 23:S24–7. https://doi.org/10.12968/bjcn.2018.23.Sup9.S24
9. Kordestani SS, 2019, Atlas of Wound Healing-E-Book: A Tissue Regeneration Approach. Amsterdam, Netherlands: Elsevier.
10. Rowan MP, Cancio LC, Elster EA, *et al*., 2015, Burn wound Healing and Treatment: Review and Advancements. *Crit Care*, 19:243. https://doi.org/10.1186/s13054-015-0961-2
11. Auger FA, Lacroix D, Germain L, 2009, Skin Substitutes and Wound Healing. *Skin Pharmacol Physiol*, 22:94–102. https://doi.org/10.1159/000178868
12. Shpichka A, Butnaru D, Bezrukov EA, *et al*., 2019, Skin Tissue Regeneration for Burn Injury. *Stem Cell Res Ther*, 10:94. https://doi.org/10.1186/s13287-019-1203-3
13. Sood A, Granick MS, Tomaselli NL, 2014, Wound Dressings and Comparative Effectiveness Data. *Adv Wound Care* (*New Rochelle*), 3:511–29. https://doi.org/10.1089/wound.2012.0401
14. Selig HF, Lumenta DB, Giretzlehner M, *et al*., 2012, The Properties of an "ideal" Burn Wound Dressing-what do we Need in Daily Clinical Practice? Results of a Worldwide Online Survey Among Burn Care Specialists. *Burns*, 38:960–6. https://doi.org/10.1016/j.burns.2012.04.007
15. Zhu Y, Ma Z, Kong L, *et al*., 2020, Modulation of Macrophages by Bioactive Glass/Sodium Alginate Hydrogel is Crucial in Skin Regeneration Enhancement. *Biomaterials*, 256:120216. https://doi.org/10.1016/j.biomaterials.2020.120216
16. Manning JH, Stark JH, 1977, Diester Crosslinked Polyglucan Hydrogels and Reticulated Sponges Thereof. Google Patents.
17. Kamoun EA, Kenawy ER, Chen X, 2017, A Review on Polymeric Hydrogel Membranes for Wound Dressing Applications: PVA-based Hydrogel Dressings. *J Adv Res*, 8:217–33. https://doi.org/10.1016/j.jare.2017.01.005
18. Lee WR, Park JH, Kim KH, *et al*., 2009, The Biological Effects of Topical Alginate Treatment in an Animal Model of Skin Wound Healing. *Wound Repair Regen*, 17:505–10. https://doi.org/10.1111/j.1524-475X.2009.00496.x
19. Abbasi AR, Sohail M, Minhas MU, *et al*., 2020, Bioinspired Sodium Alginate Based Thermosensitive Hydrogel Membranes for Accelerated Wound Healing. *Int J Biol Macromol*, 155:751–65. https://doi.org/10.1016/j.ijbiomac.2020.03.248
20. Etxabide A, Vairo C, Santos-Vizcaino E, *et al*., 2017, Ultra Thin Hydro-films Based on Lactose-crosslinked Fish Gelatin for Wound Healing Applications. *Int J Pharm*, 530:455–67. https://doi.org/10.1016/j.ijpharm.2017.08.001
21. Afjoul H, Shamloo A, Kamali A, 2020, Freeze-gelled Alginate/Gelatin Scaffolds for Wound Healing Applications: An *In Vitro, In Vivo* Study. *Mater Sci Eng C Mater Biol Appl*, 113:110957. https://doi.org/10.1016/j.msec.2020.110957
22. Augustine R, 2018, Skin Bioprinting: A Novel Approach for Creating Artificial Skin from Synthetic and Natural Building Blocks. *Prog Biomater*, 7:77–92. https://doi.org/10.1007/s40204-018-0087-0
23. Velasquillo C, Galue EA, Rodriquez L, *et al*., 2013, Skin 3D Bioprinting. Applications in Cosmetology. *J Cosmet Dermatol Sci Appl*, 3:85–9.
24. He P, Zhao J, Zhang J, *et al*., 2018, Bioprinting of Skin Constructs for Wound Healing. *Burns Trauma*, 6:5. https://doi.org/10.1186/s41038-017-0104-x
25. Fayyazbakhsh F, Leu MC, 2020, A Brief Review on 3D Bioprinted Skin Substitutes. *Procedia Manuf*, 48:790–6. https://doi.org/10.1016/j.promfg.2020.05.115
26. Ding H, Chang RC, 2018, Simulating Image-guided *In Situ* Bioprinting of a Skin Graft Onto a Phantom Burn Wound Bed. *Addit Manuf*, 22:708–19. https://doi.org/10.1016/j.addma.2018.06.022
27. Navarro J, Clohessy RM, Holder RC, *et al*., 2020, *In Vivo* Evaluation of Three-dimensional Printed, Keratin-based Hydrogels in a Porcine Thermal Burn Model. *Tissue Eng Part A*, 26:265–78. https://doi.org/10.1089/ten.TEA.2019.0181

28. Desanlis A, Albouy M, Rousselle P, *et al*., 2021, Validation of an Implantable Bioink Using Mechanical Extraction of Human Skin Cells: First Steps to a 3D Bioprinting Treatment of Deep Second Degree Burn. *J Tissue Eng Regen Med*, 15:37–48. https://doi.org/10.1002/term.3148
29. Teoh JH, Mozhi A, Sunil V, *et al*., 2021, 3D Printing Personalized, Photocrosslinkable Hydrogel Wound Dressings for the Treatment of Thermal Burns. *Adv Funct Mater*, 31:2105932. https://doi.org/10.1002/adfm.202105932
30. Pirayavaraporn C, Rades T, Tucker IG, 2012, Determination of Moisture Content in Relation to Thermal Behaviour and Plasticization of Eudragit RLPO. *Int J Pharm*, 422:68–74. https://doi.org/10.1016/j.ijpharm.2011.10.028
31. Legrand M, Barraud D, Constant I, *et al*., 2020, Management of Severe Thermal Burns in the Acute Phase in Adults and Children. Anaesth Crit Care Pa, 39:253–67. https://doi.org/10.1016/j.accpm.2020.03.006
32. Schaefer TJ, Lopez ON, 2020, Burn Resuscitation and Management. Treasure Island, FL: StatPearls Publishing.
33. Altavilla D, Saitta A, Cucinotta D, *et al*., 2001, Inhibition of Lipid Peroxidation Restores Impaired Vascular Endothelial Growth Factor Expression and Stimulates Wound Healing and Angiogenesis in the Genetically Diabetic Mouse. *Diabetes*, 50:667–74. https://doi.org/10.2337/diabetes.50.3.667
34. Xing Q, Yates K, Vogt C, *et al*., 2014, Increasing Mechanical Strength of Gelatin Hydrogels by Divalent Metal Ion Removal. *Sci Rep*, 4:4706. https://doi.org/10.1038/srep04706
35. Gao T, Gillispie GJ, Copus JS, *et al*., 2018, Optimization of Gelatin-alginate Composite Bioink Printability Using Rheological Parameters: A Systematic Approach. *Biofabrication*, 10:034106. https://doi.org/10.1088/1758-5090/aacdc7
36. Wang Y, Müller WD, Rumjahn A, *et al*., 2020, Parameters Influencing the Outcome of Additive Manufacturing of Tiny Medical Devices Based on PEEK. *Materials* (*Basel*), 13:466. https://doi.org/10.3390/ma13020466
37. Chimene D, Kaunas R, Gaharwar AK, 2020, Hydrogel Bioink Reinforcement for Additive Manufacturing: A Focused Review of Emerging Strategies. *Adv Mater*, 32:1902026. https://doi.org/10.1002/adma.201902026
38. Zhao Y, Hu F, Evans JJ, *et al*., 2011, Study of Sol-gel Transition in Calcium Alginate System by Population Balance Model. *Chem Eng Sci*, 66:848–58. https://doi.org/10.1016/j.ces.2010.11.025
39. Zou Z, Zhang B, Nie X, *et al*., 2020, A Sodium Alginate-based Sustained-release Ipn Hydrogel and its Applications. *RSC Adv*, 10:39722–30. https://doi.org/10.1039/D0RA04316H
40. Koehler J, Brandl FP, Goepferich AM, 2018, Hydrogel Wound Dressings for Bioactive Treatment of Acute and Chronic Wounds. *Eur Polym J*, 100:1–11. https://doi.org/10.1016/j.eurpolymj.2017.12.046
41. Pawlaczyk M, Lelonkiewicz M, Wieczorowski M, 2013, Age-dependent Biomechanical Properties of the Skin. *Postepy Dermatol Alergol*, 30:302–6. https://doi.org/10.5114/pdia.2013.38359
42. Aprilliza M, Editor. 2017, Characterization and Properties of Sodium Alginate from Brown Algae Used as an Ecofriendly Superabsorbent. IOP Conference Series: Materials Science And Engineering. Bristol, United Kingdom: IOP Publishing.
43. Dalal SR, Hussein MH, El-Naggar NEA, *et al*., 2021, Characterization of Alginate Extracted from *Sargassum latifolium* and its Use in *Chlorella vulgaris* Growth Promotion and Riboflavin Drug Delivery. *Sci Rep*, 11:1–17.
44. Sarker B, Papageorgiou DG, Silva R, *et al*., 2014, Fabrication of Alginate-gelatin Crosslinked Hydrogel Microcapsules and Evaluation of the Microstructure and Physico-chemical Properties. *J Mater Chem B*, 2:1470–82. https://doi.org/10.1039/C3TB21509A
45. Lim J, Shameli K, Ibrahim N, *et al*., 2011, Synthesis of Silver Nanoparticles in Chitosan, Gelatin and Chitosan/Gelatin Bionanocomposites by a Chemical Reducing Agent and their Characterization. *Molecules*, 16:7237–48. https://doi.org/10.3390/molecules16097237
46. Srinivasan P, Gottam R, 2018, Infrared Spectra: Useful Technique to Identify the Conductivity Level of Emeraldine form of Polyaniline and Indication of Conductivity Measurement Either Two or Four Probe Technique. *Mater Sci Res India*, 15:209–17.
47. Bao SP, Tjong SC, Tang CY, 2010, 8-Crystallization Behavior of Semicrystalline Polymer–Clay Nanocomposites. In: Tjong SC, Mai YW, editors. Physical Properties and Applications of Polymer Nanocomposites. Sawston, United Kingdom: Woodhead Publishing. p280–314.
48. Nagoba BS, Suryawanshi NM, Wadher B, *et al*., 2015, Acidic Environment and Wound Healing: A Review. *Wounds Compend Clin Res Pract*, 27:5–11.
49. Kulig D, Zimoch-Korzycka A, Jarmoluk A, *et al*., 2016, Study on Alginate-chitosan Complex formed with Different Polymers Ratio. *Polymers* (*Basel*), 8:167. https://doi.org/10.3390/polym8050167

50. Wang F, Li Y, Shen Y, *et al*., 2013, The Functions and Applications of RGD in Tumor Therapy and Tissue Engineering. *Int J Mol Sci*, 14:13447–62. https://doi.org/10.3390/ijms140713447

51. Kim AY, Kim Y, Lee SH, *et al*., 2017, Effect of Gelatin on Osteogenic Cell Sheet Formation Using Canine Adipose-derived Mesenchymal Stem Cells. *Cell Transplant*, 26:115–23. https://doi.org/10.3727/096368916X693338

52. Singer AJ, Boyce ST, 2017, Burn Wound Healing and Tissue Engineering. *J Burn Care Res*, 38:e605–13. https://doi.org/10.1097/bcr.0000000000000538

53. Benson A, Dickson WA, Boyce DE, 2006, ABC of Wound Healing: Burns. *BMJ*, 332:649–52.

54. Jones K, 2015, Fibrotic Response to Biomaterials and All Associated Sequence of Fibrosis. Host Response to Biomaterials. Amsterdam, Netherlands: Elsevier, p189–237.

Publisher's note